Water Supply

IWA PUBLISHING

Water Supply Vol 23 No 9, 3950 doi: 10.2166/ws.2023.210

The effect of soil porosity size distribution on integral energy content of water in different moisture slopes

Liuben Dai[a] and Zhaolei Xu[b,*]

[a] School of Civil Engineering and Architecture, Hubei University of Technology, Wuhan, Hubei 430068, China
[b] Chongqing Institute of Geology and Mineral Resources, Chongqing 404100, China
*Corresponding author. E-mail: 13368185521@163.com

ABSTRACT

The water required by the plant is provided through the porous environment of the soil around the root. Therefore, indicators such as soil texture and effective porosity have been defined to measure the amount of water available to the plant. The pore size determines water energy and the plant's ability to absorb moisture, which is evaluated in this article. Multivariate regression analysis between the integral energy of water in different ranges of humidity as the dependent variable and the indices of soil pore size distribution as the independent variable has been investigated. Due to the fact that none of the indices of the pore size distribution curve have a significant relationship with the integral energy value of water in the permanent wilting point, therefore, it was not possible to estimate this index using the indices of the pore size distribution curve. The results showed that the elongation index of soil pore size distribution curve is the only factor determining the amount of integral energy of water in different soil water contents.

Key words: integral water capacity, multivariate regression analysis, soil moisture characteristic

HIGHLIGHTS

- The effect of soil porosity size distribution on integral energy content of soil water has been considered.
- There is no significant statistical relationship with the values of integral energy of water in different humidity ranges.

INTRODUCTION

Simulation of soil water dynamics in field conditions becomes necessary to understand changes of soil water conditions to develop irrigation guidelines (Birendra *et al.* 2021; He *et al.* 2021; Hodges *et al.* 2022). The bell-shaped curve of soil pore size distribution is the result of plotting the slope of the soil moisture curve versus the equivalent diameter of the pore in a logarithmic scale (Malicki *et al.* 1992). This is in the condition that the curve is drawn based on the volumetric soil moisture against the natural logarithm of matric suction (Badr & Abuarab 2013; Lal *et al.* 2017; Qiu *et al.* 2023). Soil moisture content has a main role in water-food-energy and ecosystem nexus (Liu 2016; Tian *et al.* 2019; Wolde *et al.* 2021).

Chen *et al.* (2022) developed three models including Auto-Regressive Integrated Moving Average (ARIMA), Back-Propagation Artificial Neural Network (BP-ANN), and Least Squares Support Vector Machine (LS-SVM) to simulate the soil water content in the 0–14 cm and 14–33 cm soil layers across the Taihu Lake region of China. Rainfall, evaporation, temperature, humidity and wind speed that affect soil water content changes were considered in the BP-ANN and LS-SVM, but not in ARIMA. The results showed that the variability of soil water content in the 0–14 cm soil layer was greater than that in 14–33 cm. Correlation coefficients of soil water content between simulations and observations were highest (0.9827) using LS-SVM in the 14–33 cm soil layer, while they were the lowest (0.7019) using ARIMA in the 0–14 cm soil layer; but no significant difference in correlation coefficient values was observed between the two soil layers with the BP-ANN model. Rostami *et al.* (2022) investigated the potential of rainfed agriculture in the ZarrinehRoud basin as this basin is one of the most important sub-basins of Urmia Lake, Iran. For this study, the remote sensing data of surface soil moisture and evapotranspiration were combined with the SWAT model using the Data Assimilation method, Ensemble Kalman Filter (EnKF). Calibration of runoff flow rate in the SWAT model showed the correlation coefficient ranging between 0.69 and 0.84 in

the calibration period (2000–2009) and between 0.64 and 0.86 in the validation period (2010–2014). The assimilation of the remote sensing data with the calibrated SWAT model showed that the model simulations for both the variables of surface soil moisture and actual evapotranspiration improved by at least 25%.

Although the total amount of water available for plants has a good correlation with the plant's performance and response, certain energy is required to absorb the unit weight of water in the soil, which justifies the ease of water absorption by the plant (Yan *et al.* 2022; Zhou *et al.* 2022; Zhu *et al.* 2023). Based on this, Minasny & McBratney (2003) presented integral energy as a standard to estimate the plant's usable water.

These researchers showed that the soil moisture curve is a suitable tool for estimating the energy required by the plant to overcome the water energy in the soil and absorb the unit weight of water (Dale *et al.* 2011; Wei *et al.* 2023). This energy is a function of the amount of water, or in other words, a function of the starting and ending points of the moisture range in the soil. Researchers believe that in similar soils in terms of the amount of usable water, which is the amount of integral energy, the growth and performance of the plant and, accordingly, the efficiency of water consumption will be different (Minasny & McBratney 2003).

The results of the studies showed that the usable water of the plant is not sensitive to the soil management method (Xu *et al.* 2022; Wei *et al.* 2023). With the increase in apparent specific gravity of the soil, the usable water of the plant remains constant due to the corresponding increase in humidity, the field capacity and the wilting point, and the effect of increasing the apparent specific gravity of the soil on the usable water of the plant is not shown (Zhang *et al.* 2023). But in the same soil, with an increase in apparent specific mass, the integral energy of water will increase (Reynolds *et al.* 2008, 2009). Asgarzadeh *et al.* (2011) believed that there is a strong and significant relationship between integral energy, integral water capacity, and suction at a point with resistance equal to 5.1 MPa, as well as between integral energy, minimum limited moisture range, and suction at a point with resistance. Subsidence equivalent to 2 MPa indicates the high dependence of integral energy on the resistance of soil subsidence in its dry range.

The texture and physical quality of the soil is one of the most important issues in improving the efficiency of water consumption in the agriculture and food security sectors. Therefore, in this study, an attempt has been made to investigate the relationship between the distribution of pore size in the soil and the amount of energy required by the plant to absorb water in different soil moisture ranges. In order to evaluate and compare the distribution curves of soil pore size, different indicators of the location and shape of the curve are used. In this regard, three indicators of mode, median and average diameter equivalent of soil porosity are considered as location indicators and three indicators of standard deviation; Skewness and Kurtosis are considered as shape indicators.

METHODOLOGY

The present research was conducted during the years 2019–2022 at the research station of Chongqing Institute of Geology and Mineral Resources in China with an average height of 244 m above sea level and geographical coordinates of 102° and 21 min to 108° and 41 min of longitude and 28° and 11 min to 34° and 27 min of latitude. The soil of this station has been classified into entisol category. Generally, the surface layer had medium to light texture. Forty-five points with different texture, structure and organic matter were selected (Xu *et al.* 2022) and different soil characteristics were prepared from 0 to 30 cm depth, including one damaged sample and one intact sample using metal cylinders with a diameter of 6 cm and a height of 8 cm. In this study, the coefficients of the soil moisture curve, by fitting the Wegner-Houghton by the particle emission optimization model to the soil moisture data in suctions of 0, 10, 20, 40, 60, 80 and 100 cm using a sand box device and suctions of 500, 1,000, 10,000 and 15,000 cm were obtained using pressure plates.

These coefficients include saturated volumetric humidity ($cm^1\ cm^{-1}$), residual volumetric humidity ($cm^1\ cm^{-1}$), the image of matric suction at the air entry point (cm^{-1}) and the shape factor. The size distribution of soil particles was measured by the two-time hydrometric method and the soil texture was measured according to the United States Department of Agriculture (USDA) classification using suitable sieves. To determine the soil resistance, a penetrometer with an accuracy of 1 cm was used with a cone with an angle of 60° and a cross section of 1 cm^2. This measurement was done three times with different moisture levels in the soil sampling locations. At the same time as each measurement, a soil sample was prepared to determine the amount of moisture and after determining the percentage of moisture by weight, using the coefficients of the moisture curve of the same soil, the suction corresponding to each value of soil resistance was determined. In order to

determine a continuous function of soil resistance, a power model in the form of Equation (1) was fitted to the obtained data:

$$P = ah^b \tag{1}$$

where P is the resistance of the soil as a function of suction (MPa), h is soil suction (cm), a and b are the experimental coefficients of the model.

In order to obtain the pore size distribution curve, the slope of the soil moisture curve and the equivalent diameter of the pore (μm) should be determined. The slope of the humidity curve and the equivalent diameter of the soil porosity were determined using the equation of capillary rise using relations Equations (2) and (3), respectively (Reynolds *et al.* 2009):

$$S_v = \frac{d(\theta_v)}{d(\ln h)} = -mn(\theta_{va} - \theta_{vr})\alpha^n h^n (1 + (\alpha h)^n)^{1-m} \tag{2}$$

$$d_e = \frac{4\gamma cos\omega}{\rho_w g h} \tag{3}$$

In these formulas, θ_v is the volumetric moisture content in matric suction h, d_e is the equivalent pore diameter (μm), γ is the surface tension of water inside equivalent pore (72.8 g s^{-2}), ρ_w is the specific weight of equivalent water (0.998 g cm^{-3}), g is the equivalent acceleration of gravity (980 centimeter per square second) and ω is the contact angle of water with soil porosity, which is considered almost equal to 0.

In order to calculate the pore size distribution indices, it is necessary to first determine the effective saturation that is varied between 0 and 1. The suction can be calculated based on the effective saturation using Equation (4) and put it in Equations (3) and (5) can be obtained to calculate the equivalent diameter of soil porosity in the corresponding effective saturation:

$$S_e = (1 + (\alpha h)^n)^{-m} \tag{4}$$

$$d_{Se} = \frac{4\alpha\gamma cos\omega}{\rho_w g \left(S_e^{\frac{-1}{m}} - 1\right)^{\frac{1}{n}}} \tag{5}$$

where S_e is the effective saturation. Based on the recent relation of median, mode, mean, standard deviation and shape coefficients of soil pore size distribution curve, it can be calculated by using Equations (6)–(11) (Reynolds *et al.* 2009):

$$d_{\text{Median}} = \frac{2980\alpha}{\left(0.5^{-\frac{1}{m}} - 1\right)^{\frac{1}{n}}} \tag{6}$$

$$d_{\text{Mode}} = \frac{2980\alpha}{\left(S_i^{\frac{-1}{m}} - 1\right)^{\frac{1}{n}}} \tag{7}$$

$$d_{\text{Mean}} = \exp\frac{\ln d_{0.16} + \ln d_{0.5} + \ln d_{0.84}}{3} \tag{8}$$

where S_i is the relative saturation at the turning point of the soil moisture curve (the peak point of the pore size distribution curve).

$$Sd = \exp\left(\left(\frac{\ln d_{0.84} - \ln d_{0.16}}{4}\right) + \left(\frac{\ln d_{0.95} - \ln d_{0.05}}{6.6}\right)\right) \tag{9}$$

$$Sk = \frac{1}{2}\left(\frac{\ln d_{0.84} + \ln d_{0.16} - 2\ln d_{0.5}}{\ln d_{0.84} - \ln d_{0.16}} + \frac{\ln d_{0.05} + \ln d_{0.95} - 2\ln d_{0.5}}{\ln d_{0.95} - \ln d_{0.05}}\right) \tag{10}$$

$$Ku = \frac{\ln d_{0.05} - \ln d_{0.95}}{2.44(\ln d_{0.25} - \ln d_{0.75})} \tag{11}$$

where Sd is a standard deviation equal to one means that the diameter of pores and pores is the same in the entire soil sample, and values greater than one indicate the existence of greater diversity in different sizes of pores and pores in the soil.

The Skewness coefficient (Sk) equal to zero indicates the log-normal distribution of the pore size, the negative elongation coefficient indicates the abundance of small pores and the positive elongation coefficient indicates the abundance of large pores in the soil sample. The Kurtosis coefficient (Ku) equal to one indicates the log-normal distribution of the pore size, and values greater than one indicate that the curve is longer in the center and its tails are longer at the two ends of the curve compared to the log-normal state, and values less than one indicate that the curve is shorter in the center and its shorter tails at both ends of the curve are normal compared to the log mode. The integral energy of water in any moisture range is the result of the integral of the absolute value of the slope of the soil moisture curve in the same moisture range (Minasny & McBratney 2003). The amount of integral energy of soil water was calculated in terms of joule/kg using the following equation:

$$E = \frac{w}{10}\int_{hi}^{hf} h\left(\prod_{i=1}^{m} w_i h\right) C(h)dh \tag{12}$$

where hi is the suction at the starting point of the humidity range (cm), hf is the suction at the end point of the humidity range (cm), w is the volumetric humidity value in the humidity range ($cm^3\ cm^{-3}$), C is the absolute value of the slope of the soil moisture curve (cm^{-1}) (Qiu *et al.* 2023; Zhu *et al.* 2023), $\omega_i(h)$ is the weighting functions (for weighting different physical limitations as a function of soil suction) and the number 10 is also used to convert the unit from centimeters to joules per kilogram.

Different humidity levels are included in the calculation of integral energy, so first the values of usable water range, minimum limited humidity range and integral water capacity were determined.

In this way, the difference in soil moisture at the field capacity point (suction 100 and 330 cm) and permanent wilting (suction 15,000 cm) was considered as usable plant water. The humidity range with the minimum limit was determined by calculating the difference between the upper limit (the smaller value between the moisture of the field capacity and the humidity of ventilation porosity of 10%) and the lower limit (the larger value between the permanent wilting humidity and the resistance of 2 MPa).

Suction at the beginning and end of the moisture range for usable water, respectively, suction at the field capacity and permanent wilting points, and for the minimum limited moisture range, suction at the upper limit and lower limit of this range is considered. Now, this upper and lower limit was different in different soil samples. In some soils, permanent wilting occurred, and in others, the resistance to subsidence was set at 2 MPa. The values of the weighting functions for the range inside these two moisture ranges were considered as 1 and outside as 0. Suction at the starting and ending points of the humidity range was also considered for the integral capacity of water by determining when one of the weighting functions will be 0 at one of the wet and dry ends. The integral water capacity index value was also calculated based on Equation (13):

$$\mathrm{ECW} = \int_{0}^{\infty}\left(\prod_{i=1}^{m} w_i h\right) C(h)dh \tag{13}$$

where $C(h)$ is the absolute slope of the soil moisture curve (cm^{-1}), and $\omega_i(h)$ is weighting functions that weight different physical limitations as a function of soil suction. If there is water by the plant, it is equal to 0 and continuously increases to 1, and when there is no limit to the absorption of water by the plant, it reaches 1.

In this study, the integral energy of water for usable plant water and humidity range with the minimum limit (field capacity in suction 100 and 330 cm (EW100 and EW330)) and the integral capacity of water are shown as CW100 and CW330, respectively. To perform integral calculations in order to determine the integral energy index value of water, a subprogram has been prepared in Python.

In order to determine the statistical relationship between the shape indices and the location of the pore size distribution curve with the integral energy of water in different humidity ranges, Pearson's correlation and multivariate linear regression were also used in Python programming.

RESULTS

The results of measuring and determining the soil texture and the amounts of sand components in the studied samples are briefly shown in Table 1. The results indicate that 36% of the studied soil samples had loam texture, 27% silty loam texture, 12% silty clay loam texture, 18% clay loam texture and 7% sandy loam texture. The specific mass and organic carbon in the studied soil samples had a range between 1.56 and 1.29 and an average of 45.1 g/cm^3 and 26–0.05 and an average of 53.0%. Using the soil moisture curve coefficients, the indices of the pore size distribution curve of the soil samples were calculated (Zhang *et al.* 2023). Table 2 briefly shows the values of the mentioned indices in the studied soil samples.

Soil texture curve

The results showed that, on average, pores with a diameter of 57 μm are the most frequent in the examined soil samples. The difference between the minimum and maximum average pore diameter of 26 μm, as well as the range of calculated standard deviation changes, indicates the diversity of pore size in the soil samples, or in other words, the presence of pores with different sizes in the studied soils.

In order to compare the shape and position of the pore size distribution curve in different soils, calculations were made for soil with loam, sandy loam, silty clay loam and clay loam textures as samples and their curves were drawn. The shape and position of the curves are shown in Figure 1 and the values of the shape and position indices of the pore size distribution curve in the mentioned soil samples are presented in Table 3. The fitted curves have been obtained by a multivariate regression method.

Integral energy

As the results showed, among the examined samples, the highest average and the lowest standard deviation (less variation in pore size) were observed in the sand texture, and the lowest average and the highest standard deviation (higher variation in pore size) were observed in the clay loam texture. The maximum, minimum and average values of integral water energy in the

Table 1 | Results of analysis of soil texture

	Sand						
	Class I	Class II	Class III	Class IV	Total	Silty	Clay
Maximum	11	13.8	14.9	23.1	38	59	34
Average	4.2	6.4	6.8	9.6	27	52	21
Minimum	1.3	2.2	2.4	3.7	21	42	14

Table 2 | Values of location and shape indices of soil pore size distribution curves

	Location index				Shape index			
Soil characteristics	Median μm	Mode μm	Mean μm	Error %	Standard deviation μm	Skewness –	Kurtosis –	Error %
Maximum	53.9	367.3	28.4	3.6	163.8	−0.26	1.18	2.4
Minimum	3.6	18.7	1.2	3.1	4.5	−0.39	1.14	2.9
Average	7.2	71.6	14.7	2.7	67.4	−0.33	1.16	1.8

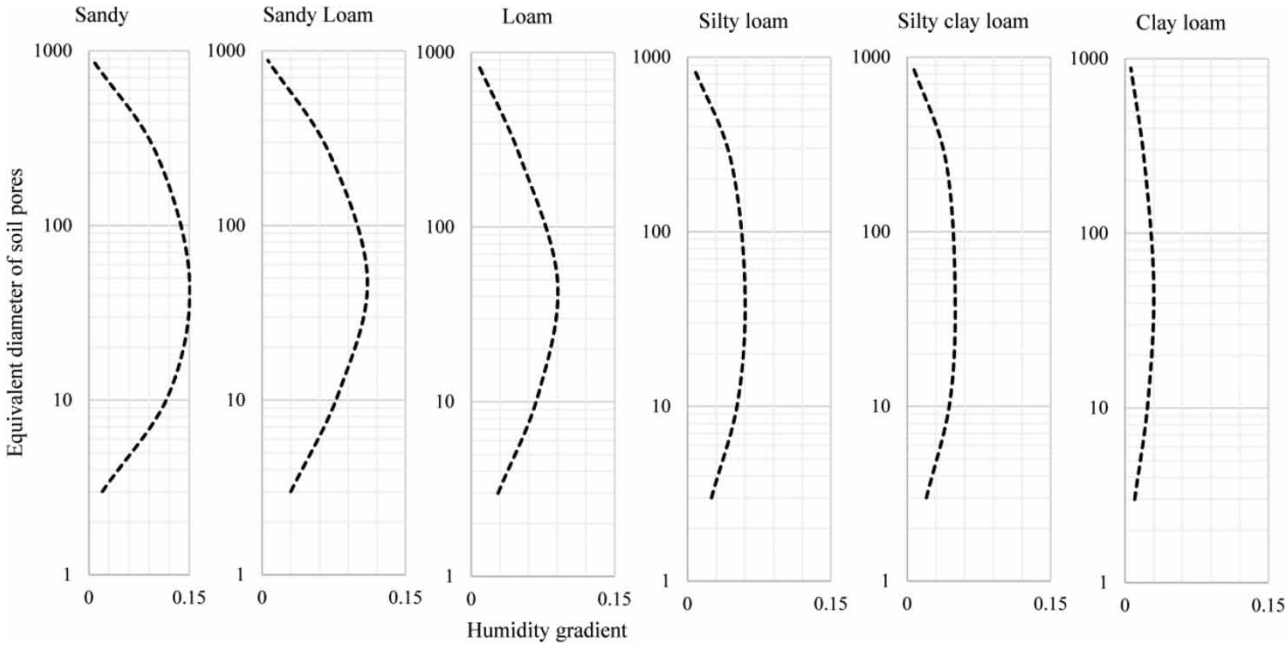

Figure 1 | Soil moisture curve.

Table 3 | Location and shape parameters of moisture curve

	Location index				Shape index			
Soil characteristics	Median μm	Mode μm	Mean μm	Error %	Standard deviation μm	Skewness –	Kurtosis –	Error %
Clay loam	1.1	46	0.36	3.7	0.23	−0.44	1.16	2.7
Silty clay loam	2.3	53	0.79	2.1	0.44	−0.41	1.14	3.5
Silty loam	4.8	61	2.34	1.8	1.28	−0.34	1.11	1.9
Loam	9.7	34	6.8	3.2	3.7	−0.27	1.17	2.4
Sandy loam	18.7	29	11.4	2.6	6.4	−0.23	1.15	2.6
Sandy	23.6	48	16.9	1.4	8.9	−0.17	1.13	3.7

range of usable water, moisture range with the minimum limit and also the integral capacity of water in the examined soil samples are presented in Figure 2. The results of the investigation of integral water energy values in different moisture ranges in the studied soils showed that on average, soils with sandy loam and silty loam texture had the lowest and soils with silty clay loam texture had the highest value of this index.

The results indicate that the average value of the integral energy of water in the humidity range with the minimum limit, in which, in addition to the humidity at the field capacity points and permanent wilting, ventilation restrictions and soil subsidence resistance, are also considered, from the average value of this factor in the water range. The usable capacity of the plant (corresponding field capacity) is less. Another noteworthy point is the average amount of integral water energy in the range of integral water capacity, which is lower than the value of this index in the humidity range.

It can be stated that the index of integral water capacity by taking into account the limitations of water absorption by the plant as a continuous function of water suction in the soil and calculating the integral energy according to the effect of these limitations, is a better measure to express the availability of water for the plant. The results of other researchers also showed that, on average, the amount of integral energy was the lowest in the range of integral water capacity and the highest in the range of plant usable water. The statistical relationship between the indices of the pore size distribution curve and the integral energy values of water in different humidity ranges is presented in the form of Pearson's correlation coefficient in Table 4.

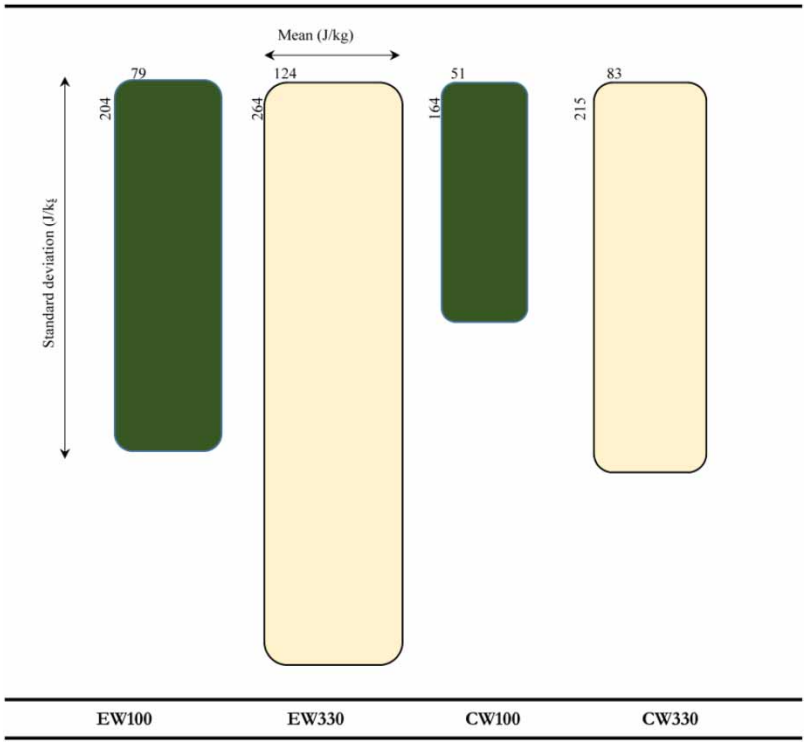

Figure 2 | Mean and standard deviation of integral energy.

Table 4 | Integral energy components

	EW100	EW330	CW100	CW330	ECW
Median	−036*	−0.26*	−0.08*	0.21*	−0.34*
Mode	0.12^{ns}	-0.07^{ns}	0.04^{ns}	0.14^{ns}	-0.07^{ns}
Mean	−0.62**	−0.34**	−0.16**	0.08**	0.37**
Standard deviation	0.54^{ns}	-0.04^{ns}	0.37^{ns}	0.14^{ns}	0.52^{ns}
Skewness	−0.84**	−0.4**	−0.41**	−0.18**	0.31**
Kurtosis	−0.34*	−0.21*	−0.27*	−0.14*	−0.36*

*Significant difference at 1%; **Significant difference at 5%; ns, no significant difference.

CONCLUSION

The results showed that the mean and mode indices of soil pore diameter have no significant statistical relationship with the values of integral energy of water in different humidity ranges. Among the three indices of soil pore size distribution curve position, only the average pore diameter index had a significant negative relationship with integral water energy in EW100, EW330 and ECW. In this regard, the elongation index also showed a negative and significant effect on the integral energy of ECW, CW100, CW330 and EW100 of water, in which the increase in the diameter of the soil pores leads to a decrease in the integral energy of water in the mentioned moisture ranges and facilitates the absorption of water by the plant. The results of the study of the relationship between the standard deviation of the pore size distribution curve or the variation of the pore size with the values of the integral energy of water in different moisture ranges showed that with the decrease of the variation of the diameter of the pores in the soil, the integral energy of water in ECW decreases. The increase in the uplift index of the soil pore size distribution curve in the studied soil samples showed a significant decrease in the integral energy of water in ECW. This means that the curve is longer in the center and its traces are longer at both ends of the curve compared to the normal log state.

ETHICS APPROVAL

This article does not contain any studies with animals performed by any of the authors.

DATA AVAILABILITY STATEMENT

All relevant data are included in the paper or its Supplementary Information.

CONFLICT OF INTEREST

The authors declare there is no conflict.

REFERENCES

Asgarzadeh, H., Mosaddeghi, M. R., Mahboubi, A. A., Nosrati, A. & Dexter, A. R. 2011 Integral energy of conventional available water, least limiting water range and integral water capacity for better characterization of water availability and soil physical quality. *Geoderma* **166**, 34–42.

Badr, A. E. & Abuarab, M. E. 2013 Soil moisture distribution patterns under surface and subsurface drip irrigation systems in sandy soil using neutron scattering technique. *Irrig. Sci.* **31**, 317–332. https://doi.org/10.1007/s00271-011-0306-0.

Birendra, K. C., Chau, H. W., Mohssen, M., Cameron, K., Safa, M., McIndoe, I., Rutter, H., Dark, A., Lee, M., Pandey, V. P., Schultz, B. & Prasad, K. 2021 Assessment of spatial and temporal variability in soil moisture using multi-length TDR probes to calibrate Aquaflex sensors. *Irrig. Sci.* **39**, 703–713. https://doi.org/10.1007/s00271-021-00747-x.

Chen, C., Lv, Q. & Tang, Q. 2022 Simulating and predicting soil water dynamics using three models for the Taihu Lake region of China. *Water Supply* **22** (4), 4030–4042. doi:10.2166/ws.2022.032.

Dale, V. H., Efroymson, R. A. & Kline, K. L. 2011 The land use–climate change–energy nexus. *Landscape Ecol.* **26**, 755–773. https://doi.org/10.1007/s10980-011-9606-2.

He, M., Dong, J., Jin, Z., Liu, C., Xiao, J., Zhang, F. & Deng, L. 2021 Pedogenic processes in loess-paleosol sediments: clues from Li isotopes of leachate in Luochuan loess. *Geochim. Cosmochim. Acta* **299**, 151–162. https://doi.org/10.1016/j.gca.2021.02.021.

Hodges, B., Tagert, M. L. & Paz, J. O. 2022 Use of a crop model and soil moisture sensors for estimating soil moisture and irrigation applications in a production soybean field. *Irrig. Sci.* **40**, 925–939. https://doi.org/10.1007/s00271-022-00802-1.

Lal, R., Mohtar, R. H. & Assi, A. T. 2017 Soil as a basic nexus tool: soils at the center of the food–energy–water nexus. *Curr. Sustain. Renew. Energy Rep.* **4**, 117–129. https://doi.org/10.1007/s40518-017-0082-4.

Liu, Q. 2016 Interlinking climate change with water-energy-food nexus and related ecosystem processes in California case studies. *Ecol. Processes* **5** (14). https://doi.org/10.1186/s13717-016-0058-0.

Malicki, M. A., Plagge, R., Renger, M. & Walczak, R. T. 1992 Application of time-domain reflectometry (TDR) soil moisture miniprobe for the determination of unsaturated soil water characteristics from undisturbed soil cores. *Irrig. Sci.* **13**, 65–72. https://doi.org/10.1007/BF00193982.

Minasny, B. & McBratney, A. B. 2003 Integral energy as a measure of soil–water availability. *Plant Soil* **249**, 253–262.

Qiu, D., Zhu, G., Lin, X., Jiao, Y., Lu, S., Liu, J. & Chen, L. 2023 Dissipation and movement of soil water in artificial forest in arid oasis areas: cognition based on stable isotopes. *CATENA* **228**, 107178. doi:10.1016/j.catena.2023.107178.

Reynolds, W. D., Drury, C. F., Yang, X. M. & Tan, C. S. 2008 Optimal soil physical quality inferred through structural regression and parameter interactions. *Geoderma* **146**, 466–474.

Reynolds, W. D., Drury, C. F., Tan, C. S., Fox, C. A. & Yang, X. M. 2009 Use of indicators and pore volume-function characteristics to quantify soil physical quality. *Geoderma* **152**, 252–263.

Rostami, A., Raeini-Sarjaz, M., Chabokpour, J., Azamathulla, H. & Kumar, S. 2022 Determination of rainfed wheat agriculture potential through assimilation of remote sensing data with SWAT model case study: ZarrinehRoud Basin, Iran. *Water Supply* **22** (5), 5331–5354. doi:10.2166/ws.2022.160.

Tian, H., Huang, N., Niu, Z., Qin, Y., Pei, J. & Wang, J. 2019 Mapping winter crops in China with multi-source satellite imagery and phenology-based algorithm. *Remote Sens.* **11** (7), 820. doi:10.3390/rs11070820.

Wei, X., Bai, X., Wen, X., Liu, L., Xiong, J. & Yang, C. 2023 A large and overlooked Cd source in karst areas: the migration and origin of Cd during soil formation and erosion. *Sci. Total Environ.* **895**, 165126. doi:10.1016/j.scitotenv.2023.165126.

Wolde, Z., Wei, W. & Likessa, D. 2021 Understanding the impact of land use and land cover change on water–energy–food nexus in the Gidabo Watershed, East African Rift Valley. *Nat. Resour. Res.* **30**, 2687–2702. https://doi.org/10.1007/s11053-021-09819-3.

Xu, Z., Wang, Y., Jiang, S., Fang, C., Liu, L., Wu, K. & Chen, Y. 2022 Impact of input, preservation and dilution on organic matter enrichment in lacustrine rift basin: a case study of lacustrine shale in Dehui Depression of Songliao Basin, NE China. *Mar. Pet. Geol.* **135**, 105386. doi:10.1016/j.marpetgeo.2021.105386.

Yan, Y., Jarvie, S., Liu, Q. & Zhang, Q. 2022 Effects of fragmentation on grassland plant diversity depend on the habitat specialization of species. *Biol. Conserv.* **275**, 109773. doi:10.1016/j.biocon.2022.109773.

Zhang, T., Song, B., Han, G., Zhao, H., Hu, Q., Zhao, Y. & Liu, H. 2023 Effects of coastal wetland reclamation on soil organic carbon, total nitrogen, and total phosphorus in China: a meta-analysis. *Land Degrad. Dev.* doi:10.1002/ldr.4687.

Zhou, J., Wang, L., Zhong, X., Yao, T., Qi, J., Wang, Y. & Xue, Y. 2022 Quantifying the major drivers for the expanding lakes in the interior Tibetan Plateau. *Sci. Bull.* **67** (5), 474–478. doi:10.1016/j.scib.2021.11.010.

Zhu, G., Liu, Y., Wang, L., Sang, L., Zhao, K., Zhang, Z. & Qiu, D. 2023 The isotopes of precipitation have climate change signal in arid Central Asia. *Global Planet. Change* **225**, 104103. doi:10.1016/j.gloplacha.2023.104103.

First received 15 June 2023; accepted in revised form 27 July 2023. Available online 14 August 2023